Barred Galaxies

Morphology
Gas in barred galaxies
Dynamics: pattern speed
Theory: secular evolution, resonances

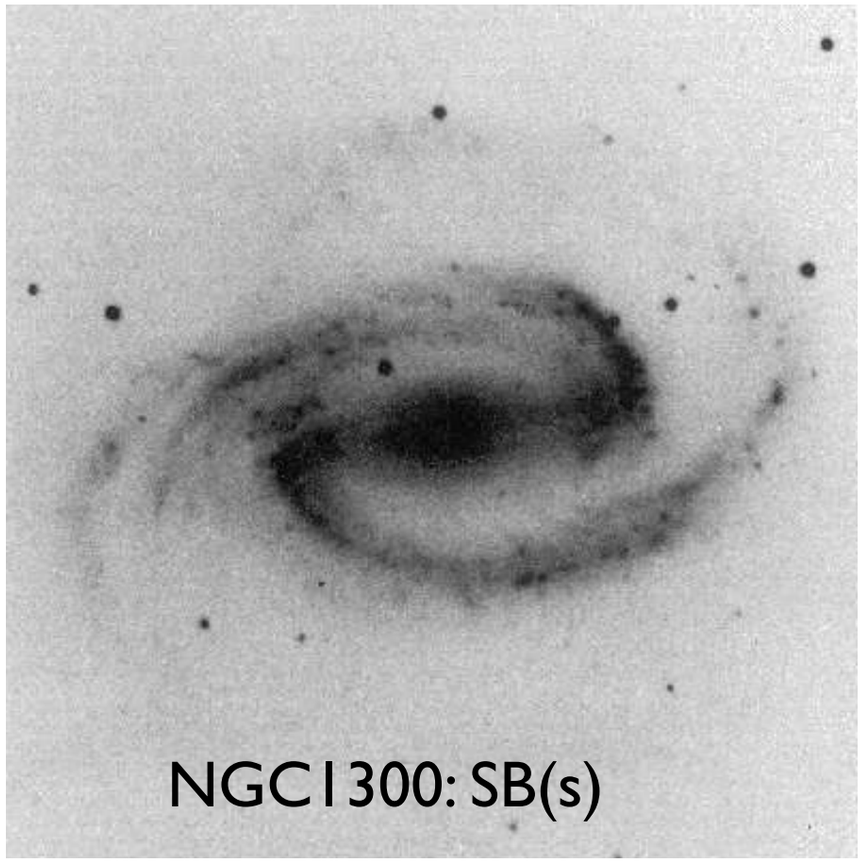

NGC1300: SB(s)

fig.6

1. Barred spiral galaxies are divided into subclasses SB(s), in which the spiral arms begin at the ends of the bar, and SB(r), in which a complete "inner ring" of stars connects the ends of the bar. In the latter case, the spiral arms start somewhere on the ring, "often downstream from the ends of the bar" (Sandage & Bedke 1994). SB(r) and SB(s) galaxies are contrasted in Figure 6; additional SB(r) galaxies are shown in Figures 3 and 5, and additional SB(s) galaxies are shown in Figure 7.
2. Some barred and oval galaxies have "outer rings" (R) that are 2.2 ± 0.1 times the diameter of the bar or inner disk. Outer rings in barred and unbarred galaxies are similar (Fig. 2, 5). Inner and outer rings are different; there is no size overlap. Some galaxies contain both (Fig. 5).

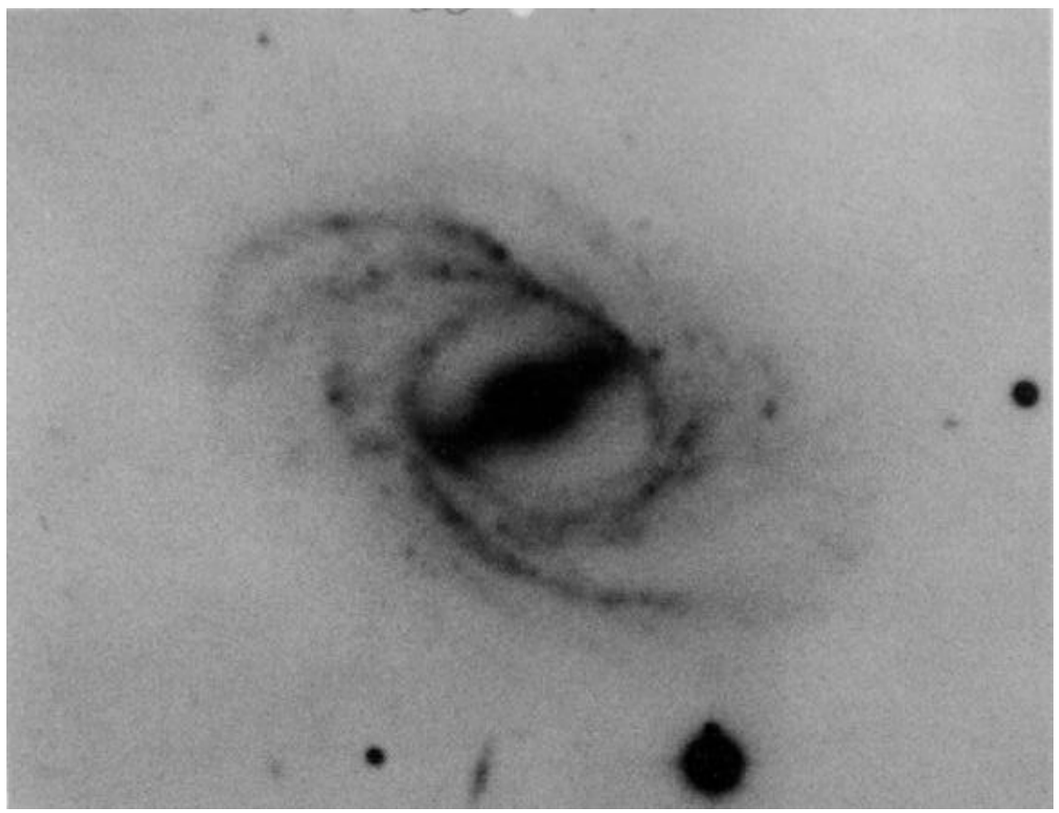

NGC2523: SB(r)

NGC1512: SB(r) fig.3

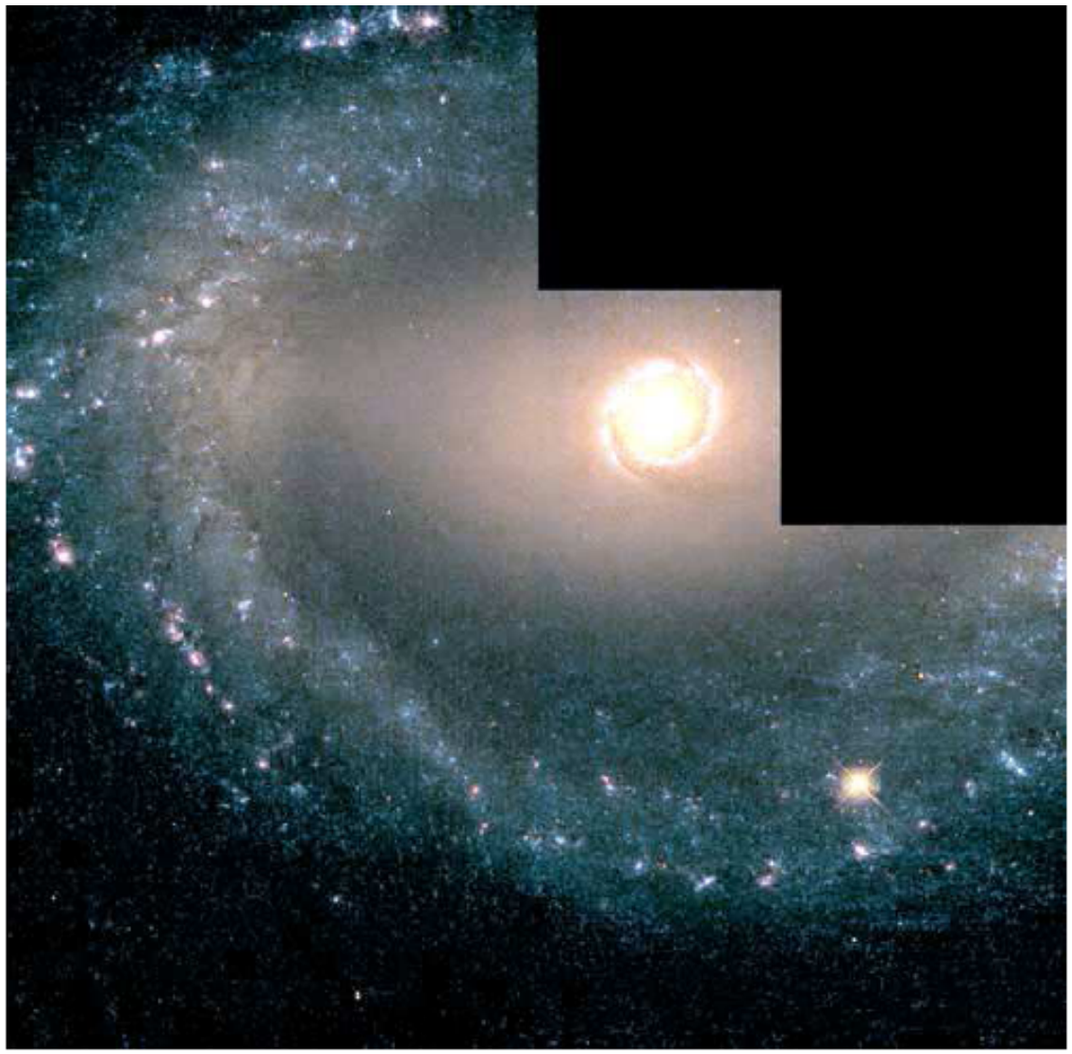

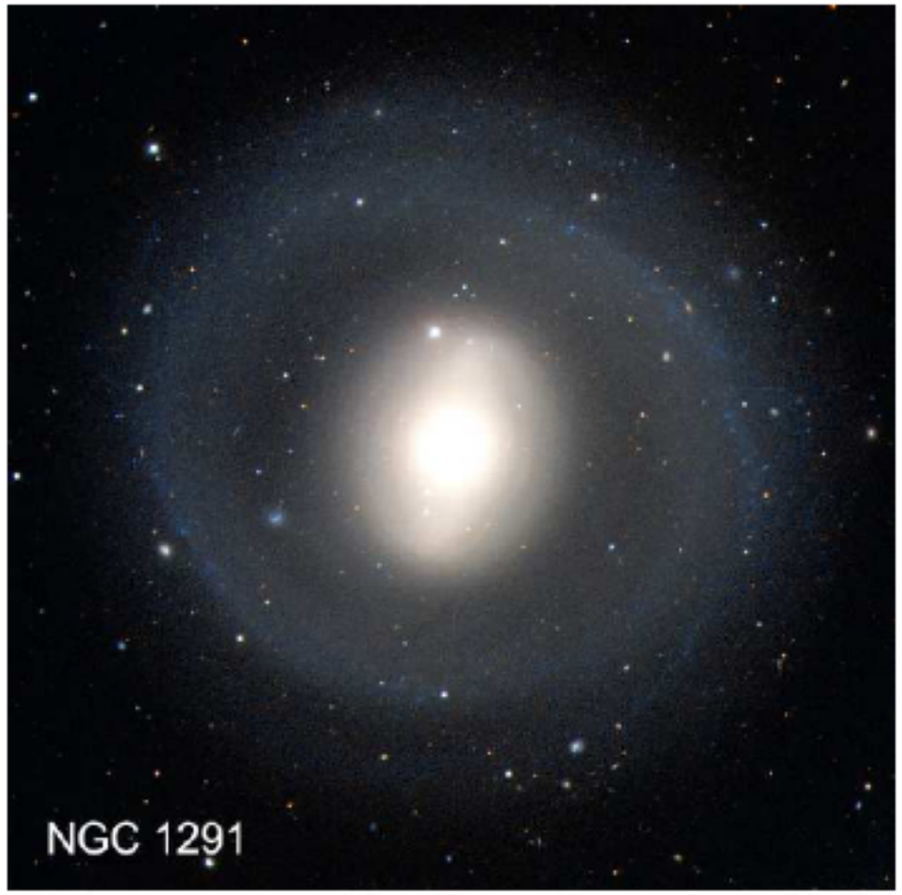

fig.2

3. At intermediate Hubble types, when the bar is made mostly of old stars and the disk contains many young stars, the stellar population of inner and outer rings is like that of the disk, not like that of the bar (Figures 2 and 3). Inner and outer rings generally contain gas.

4. In SB(s) galaxies, an almost-straight dust lane parallels the ridge line of the bar but is displaced slightly forward in the direction of galactic rotation. Such dust lanes are analogous to and connect up with the prominent dust lanes seen on the trailing side of the arms in global-pattern spirals. Examples are shown in Figures 6, 7, and 8. These dust lanes are almost never present in SB(r) galaxies (Sandage 1961). NGC 1512 in Figure 3 is a rare exception.

5. Many barred and oval galaxies have very active star formation near their centers, in what is conventionally identified as the bulge. Often the star formation is concentrated in a ring. Figures 3, 7, and 8 show examples.

6. Many barred galaxies have "bulges" that are themselves elongated into a structure resembling a bar. Examples are shown in Figure 14.

7. Many early-type SB galaxies contain a "lens" in the disk – a shelf of slowly decreasing surface brightness with a sharp outer edge. Lenses have intrinsic axial ratios of ~ 0.85; the bar usually fills the longest dimension. These properties are discussed in Kormendy (1979a, b, 1981, 1982a) and in Athanassoula et al. (1982). Lenses are sometimes seen in unbarred galaxies; NGC 1553 is the best example (Freeman 1975; Kormendy 1984). Lenses in early-type galaxies look similar to oval disks in late-type galaxies (Section 3.2); it is not clear whether or not they are physically similar. Lenses are illustrated in Figures 2 and 5.

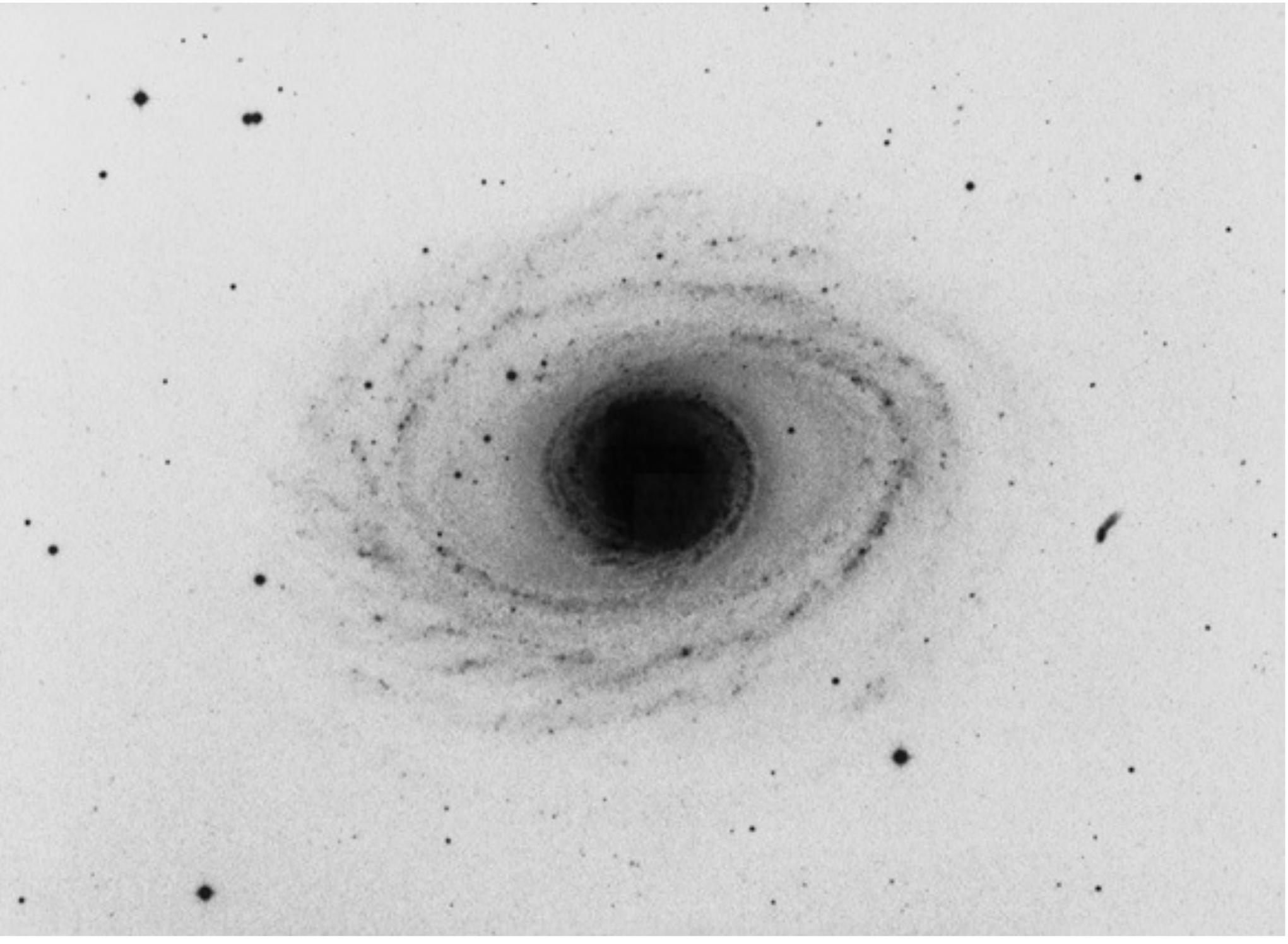

NGC 1398

Looks like a normal spiral galaxy

NGC 1398

With shorter exposure we clearly see the bar.

This is actually a spiral bared galaxy.
We cannot see the outer parts of the galaxy because the levels of surface brightness are relatively high. However, the central region is clearly resolved.

NGC 1300

- Dust lanes
- Star formation regions
- Old stellar bar

Barred Galaxies: overall properties

- Barred galaxies are numerous: 1/3 of all spirals have strong bars and 1/3 has a weaker inner bar
- Our Galaxy and Andromeda are barred galaxies
- LMC is a barred galaxy
- Typically star formation inside the bar is suppressed (but not in nucleus)
- Barred galaxies sometimes have rings: inner and outer rings
- Length of a bar is typically close to the exponential scale-length of the disk. Yet, there is substantial spread
- Bars have boxy shape:

  $(x/a)^c + (y/b)^c = 1$ with $c=2.5\text{-}5.5$

- Bars rotate, with a pattern speed that is close to the angular circular speed in the disk near the bar ends. If R_{bar} is the radius of the bar and $R_{corotation}$ is the radius of corotation, than:

  $$R_{bar} \approx R_{corotation} / 1.3$$

Morphology of surface brightness profiles

- Early Type: flat inner profile

- Late Type: double exponential

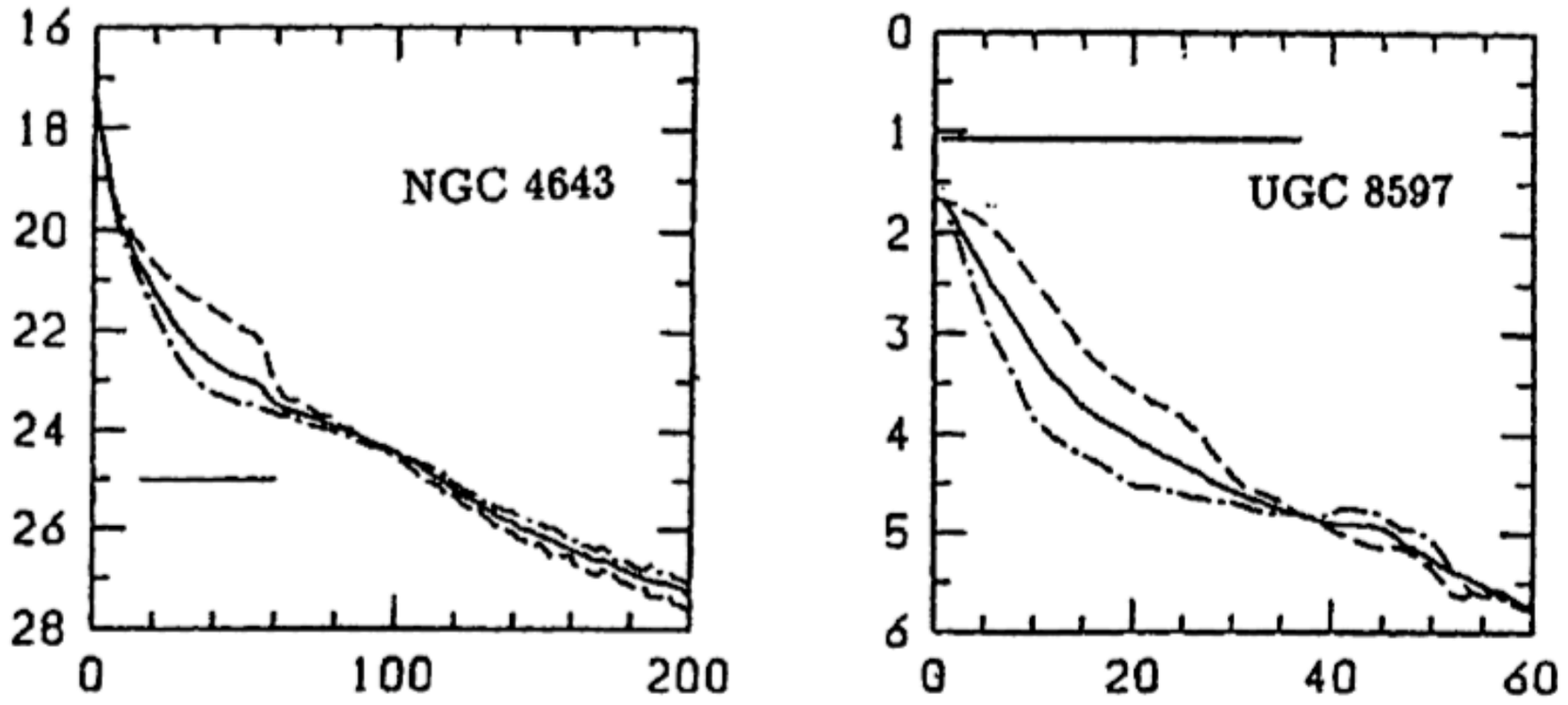

Figure 3. Radial profiles of an early-type (left panel) and a late-type (right panel) barred galaxy. The ordinate is surface brightness in magnitude scale and the abscissa is radius in arcsec. Solid lines, dashed lines, and dot-dashed lines represent azimuthally averaged profiles, profiles along the bar major axis, and profiles along the bar minor axis, respectively. A horizontal line in each panel shows the bar region.

NGC1512: SB(r): Central active region

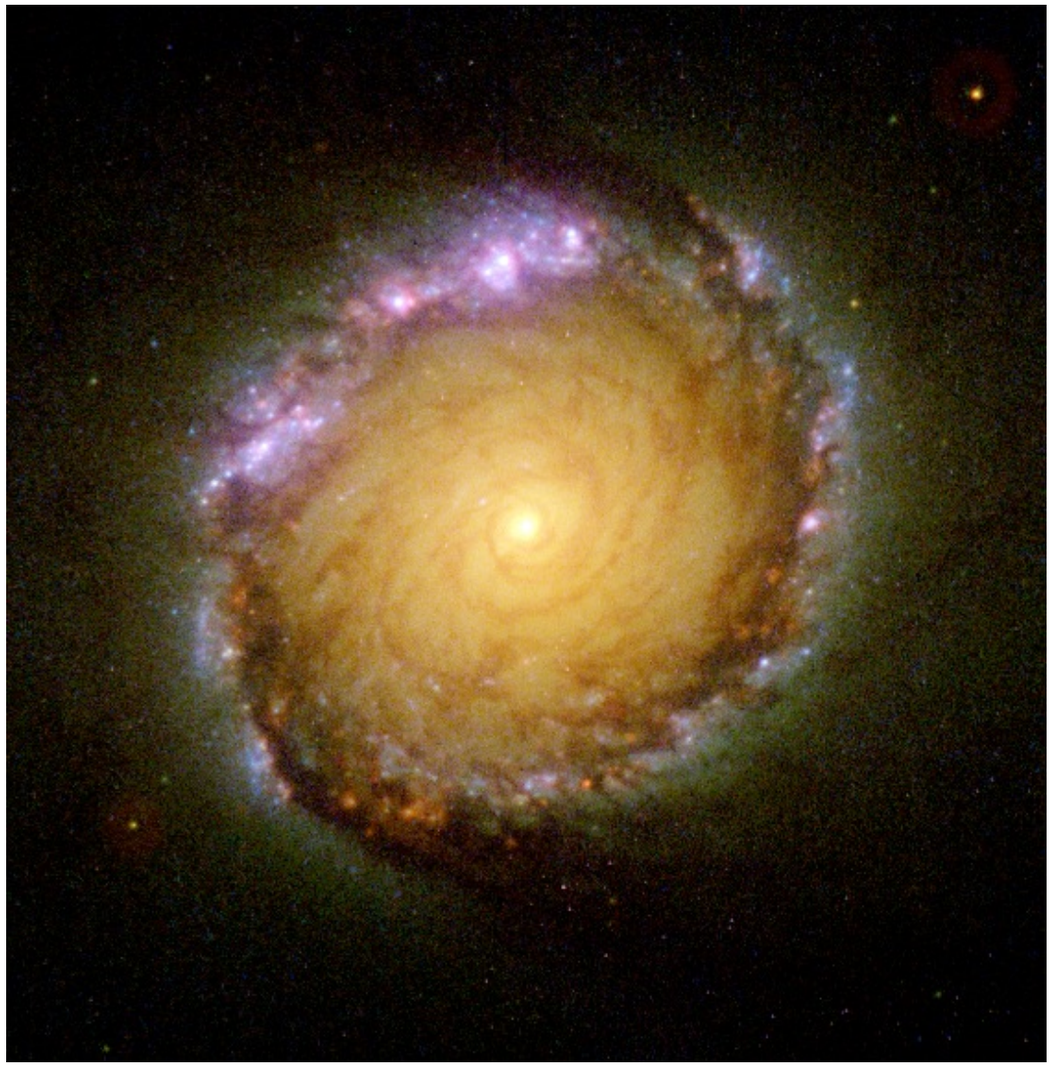

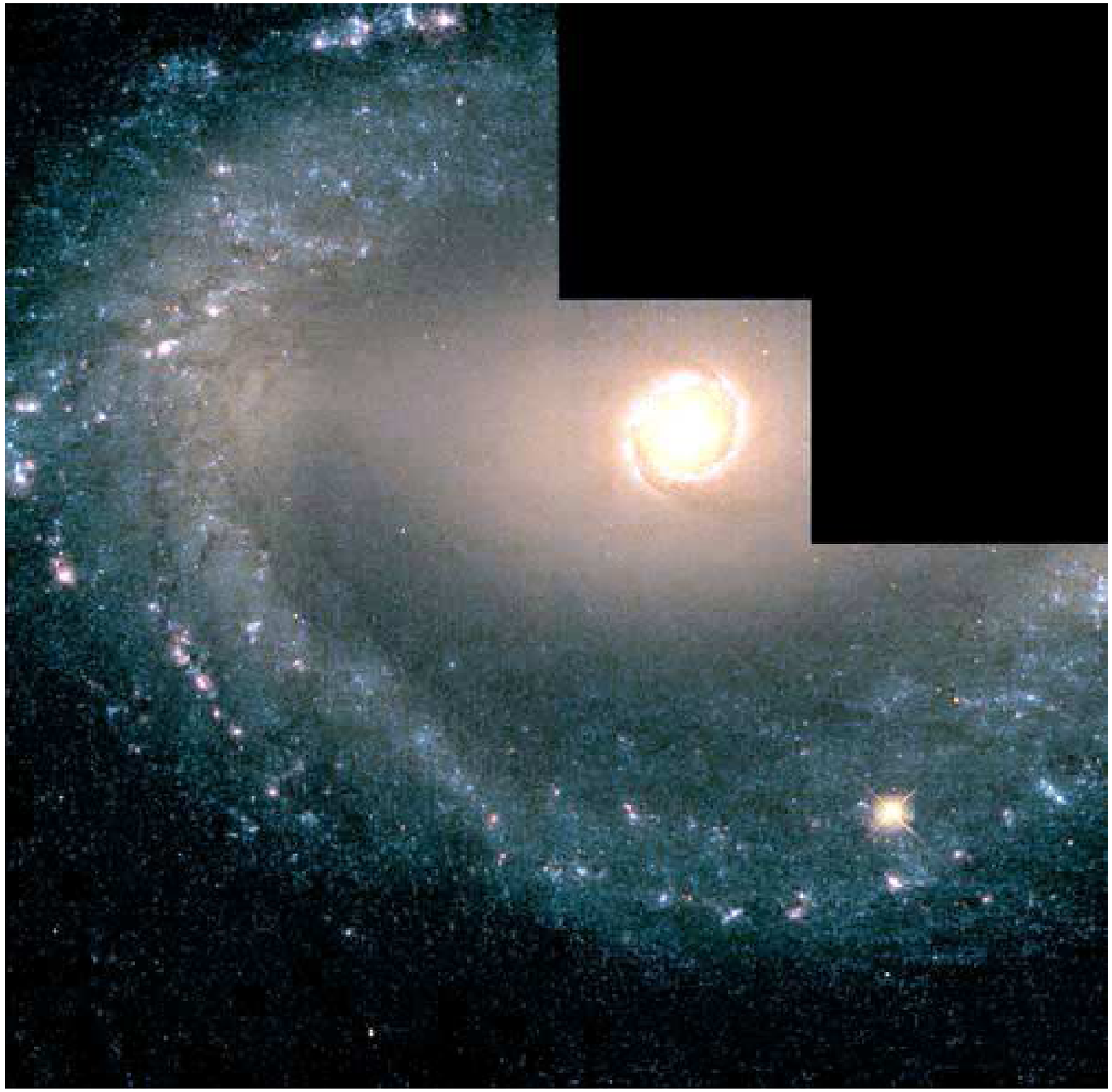

Motion of Gas

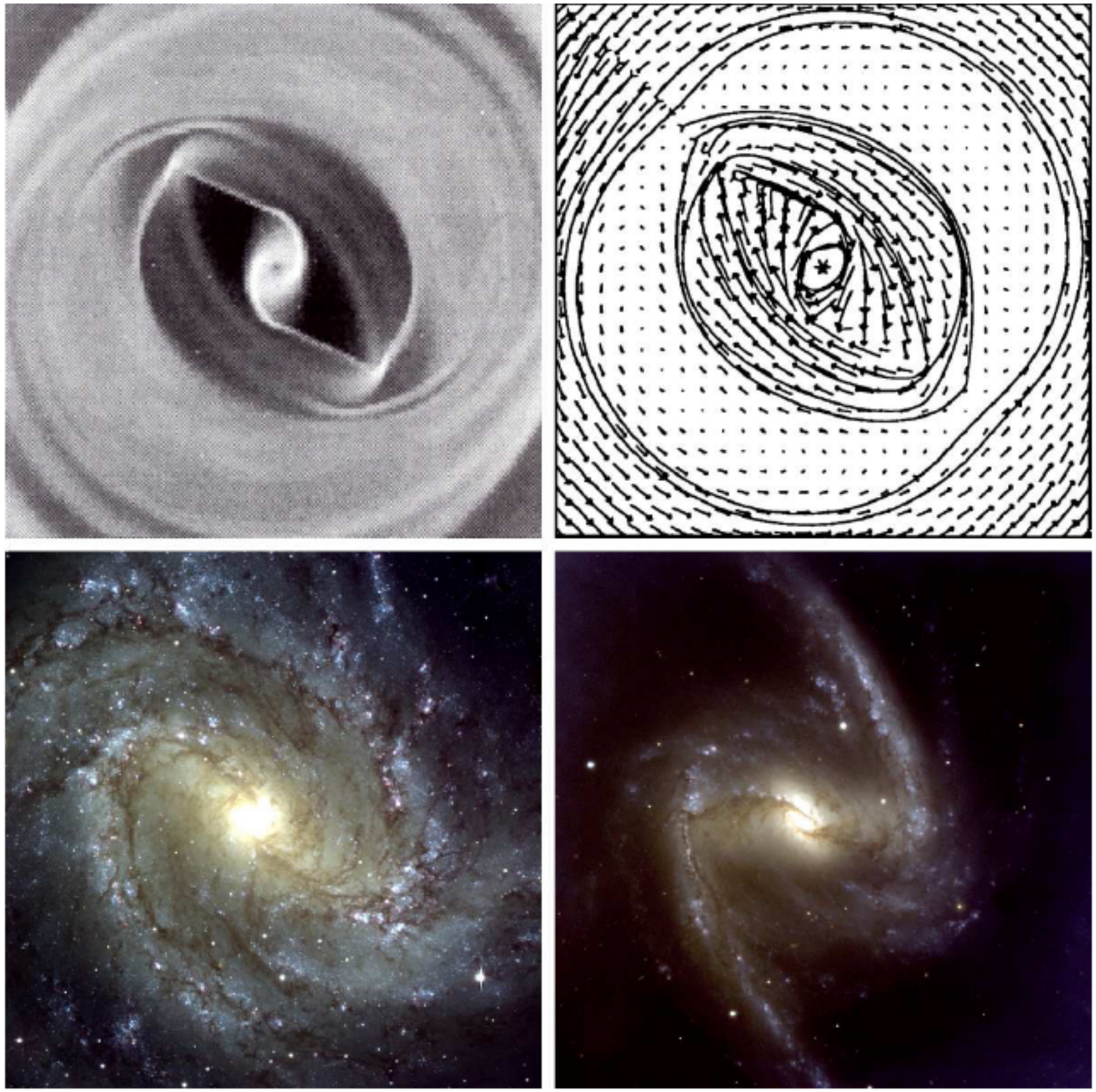

Figure 7 Comparison of the gas response to a bar (Athanassoula 1992b model 001) with NGC 5236 (left) and NGC 1365 (right). The galaxy images

Nuclear bars

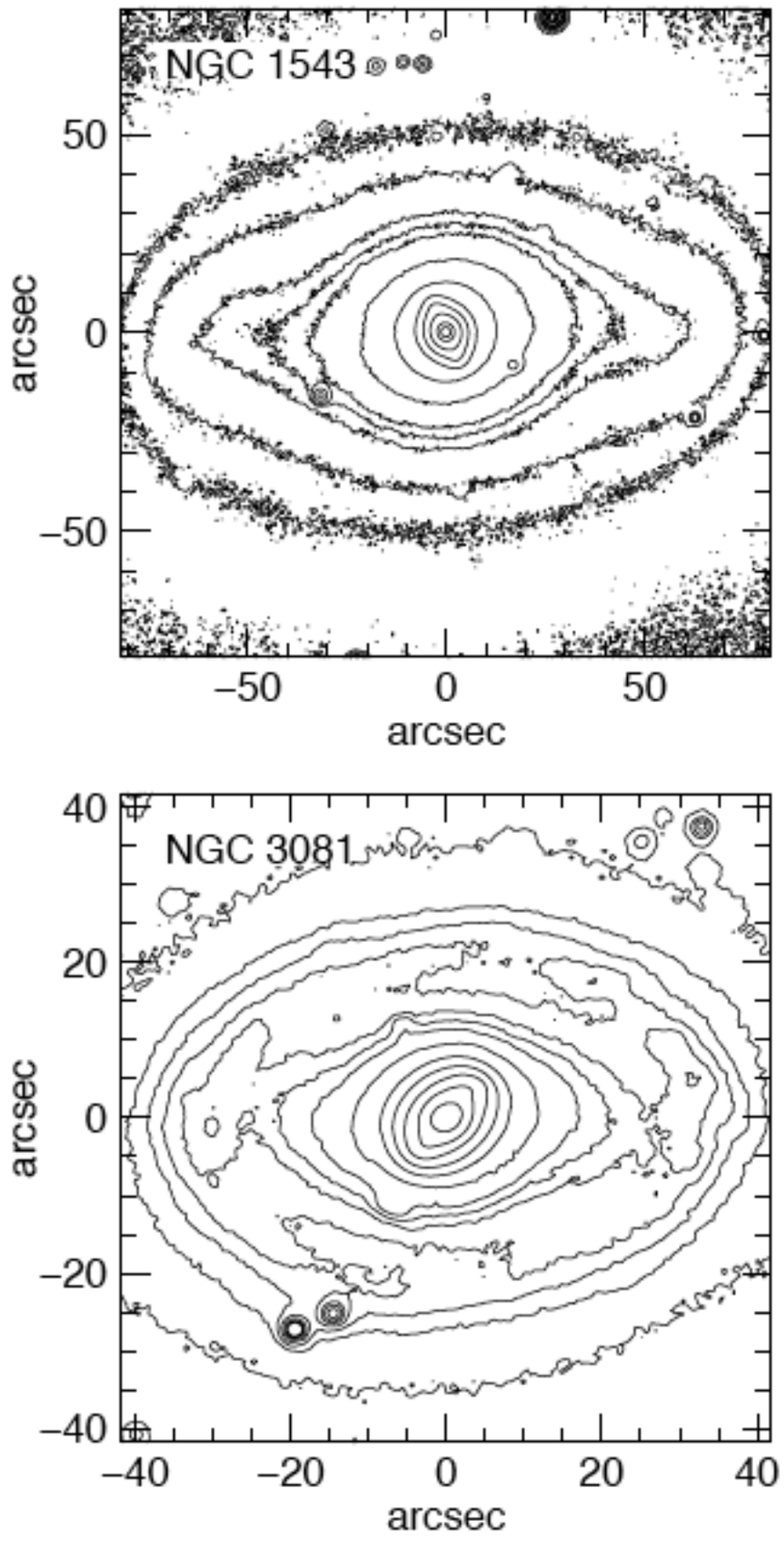

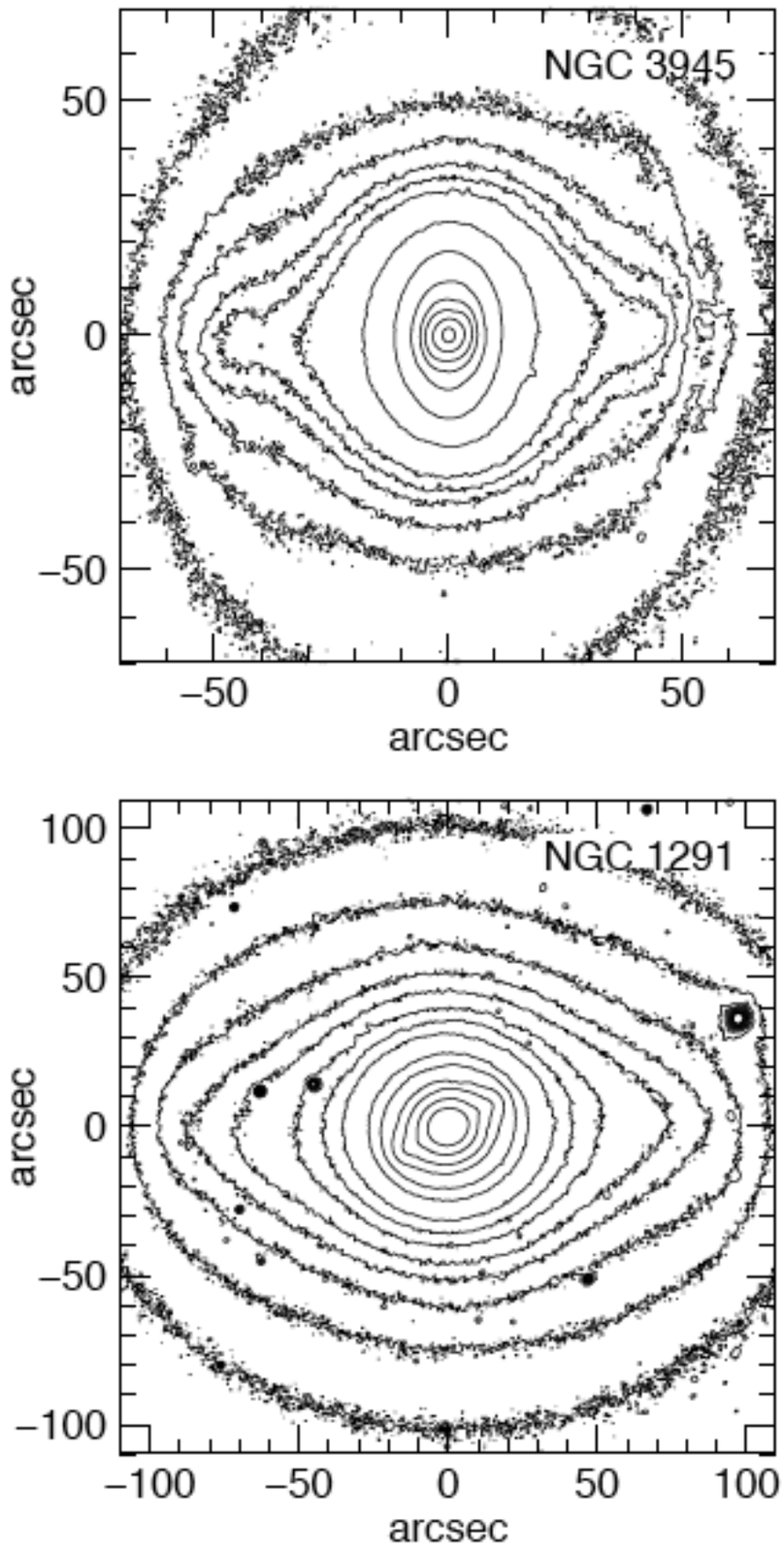

Peanut-shape bulges are signatures of barred galaxies

This unusual looking galaxy is a spiral barred galaxy viewed edge-on. Note the x-shaped central bulge.

Peanut-shape bulges: sign of a bar

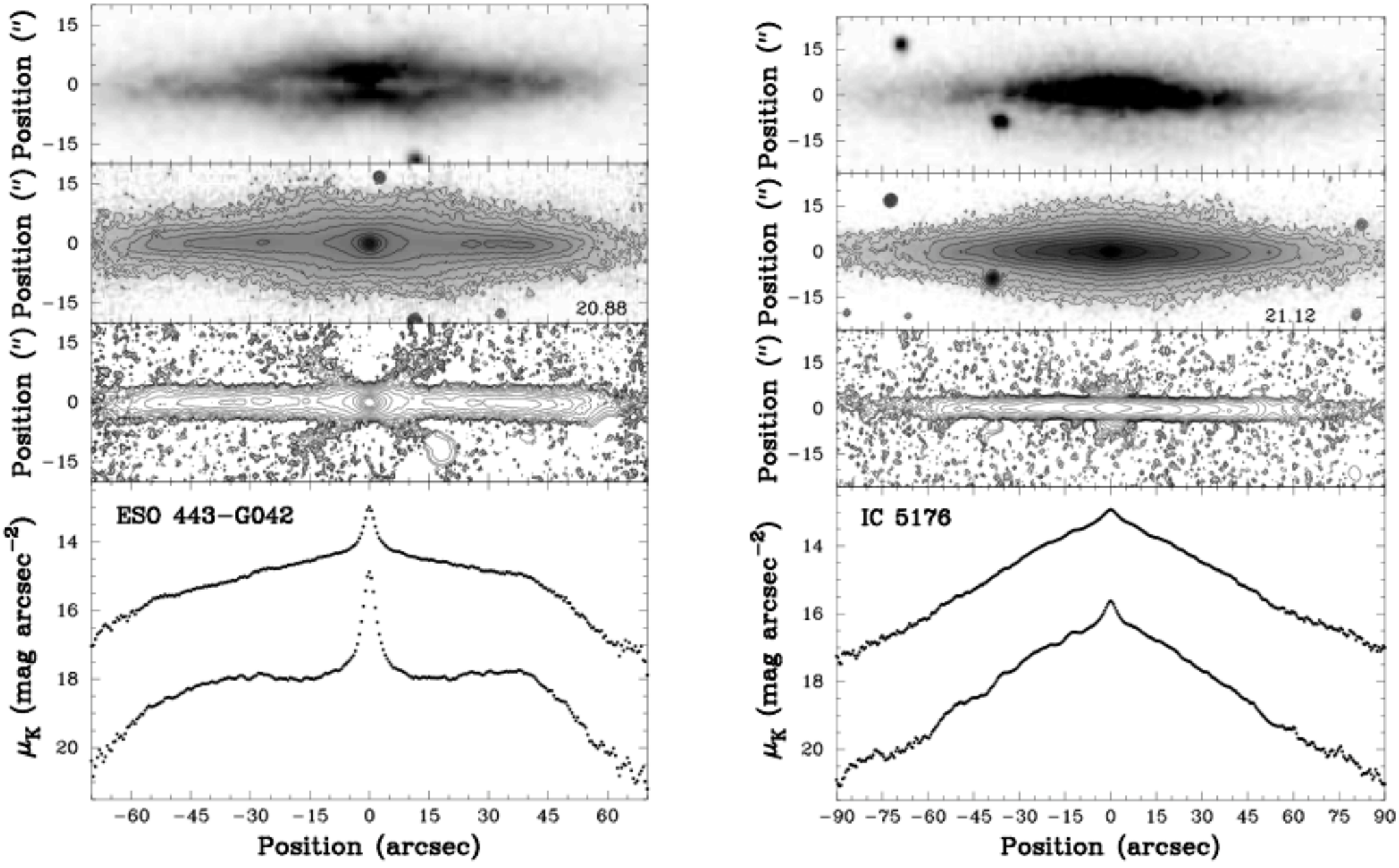

Figure 1. Images and surface brightness profiles of the galaxies ESO443-G042 (left), with a B/PS bulge, and IC5176 (right), with a nearly pure disc. From top to bottom, each panel shows first a DSS image of the galaxy, second our *K*n-band image, third an unsharp-masked *K*n-band image, and last the major-axis (fainter) and vertically-summed (brighter) surface brightness profiles, all spatially registered.

Azimuthal variations of surface brightness

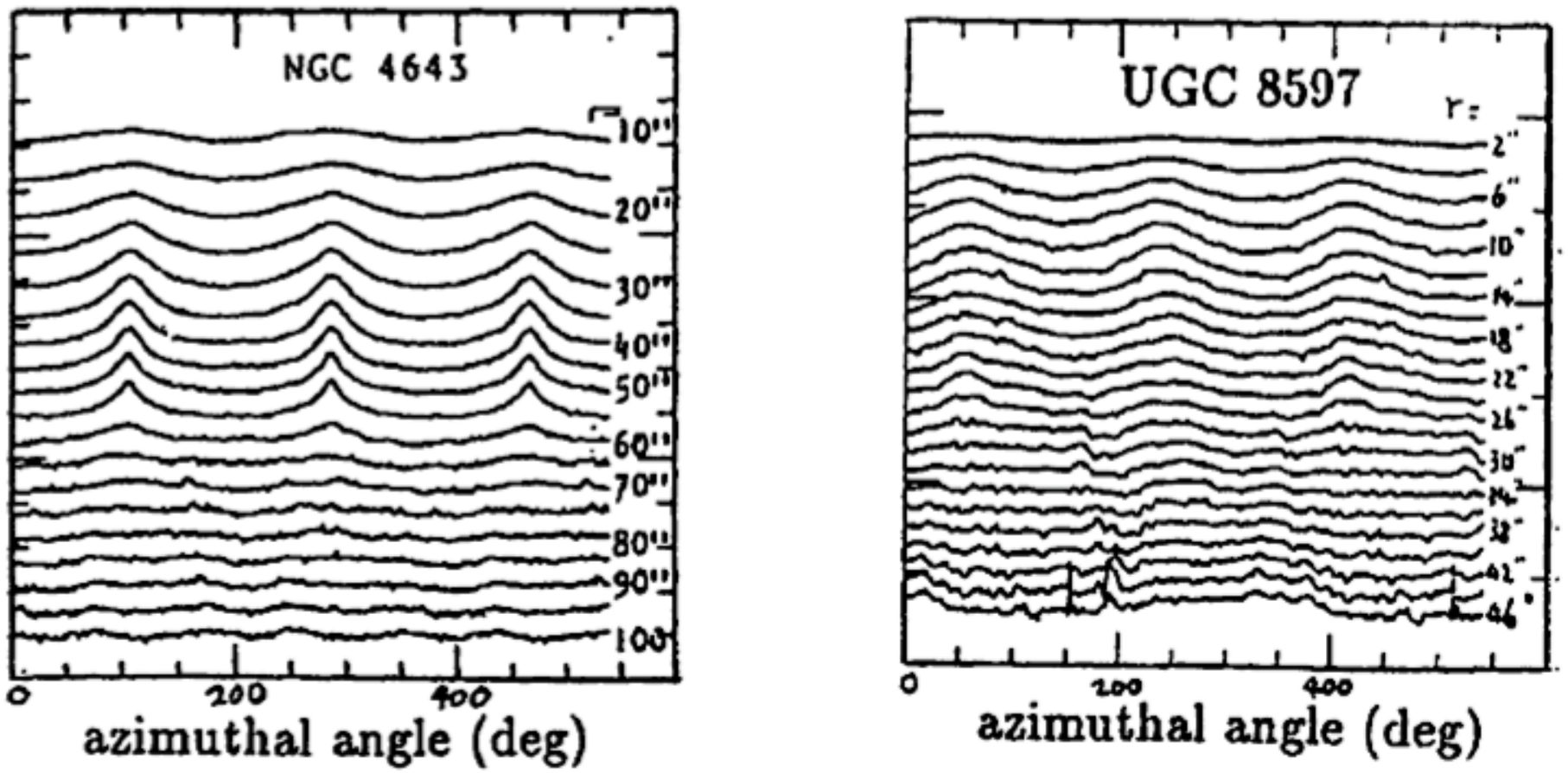

Figure 1. Azimuthal profiles of an early-type (left panel) and a late-type (right panel) barred galaxy. The ordinate and the abscissa are surface brightness in arbitrary units and azimuthal angle, respectively. The upper part in each panel shows profiles in the bulge region, the middle part shows profiles in the bar region, and the lower part shows profiles in the outer disk region.

Unlike spiral arms, bars have very large variations of the stellar mass: a factor of 2-3 for innner/out bar regions

Figure 2 shows the results of the Fourier decomposition. The Fourier components are defined as follows,

$$I(r,\theta) = A_0(r)/2 + \sum_m [A_m(r)\cos m\theta + B_m(r)\sin m\theta],$$

where

$$A_m(r) = \frac{1}{\pi}\int_0^{2\pi} I(r,\theta)\cos m\theta \mathrm{d}\theta, \quad \text{and} \quad B_m(r) = \frac{1}{\pi}\int_0^{2\pi} I(r,\theta)\sin m\theta \mathrm{d}\theta.$$

The Fourier amplitude of the m-th component is defined as

$$I_0(r) = A_0(r)/2, \quad I_m(r) = [A_m(r)^2 + B_m(r)^2]^{1/2},$$

and the relative amplitude of the m-th component is defined as $I_m(r)/I_0(r)$. In both early- and late-type barred galaxies, the amplitudes of the m=2 component are the largest, but in the early-type barred galaxies the contributions of m=4, m=6, and m=8 components are also large, while in the late-type barred galaxies only the amplitudes of m=4 are significant and contributions from higher components are negligible.

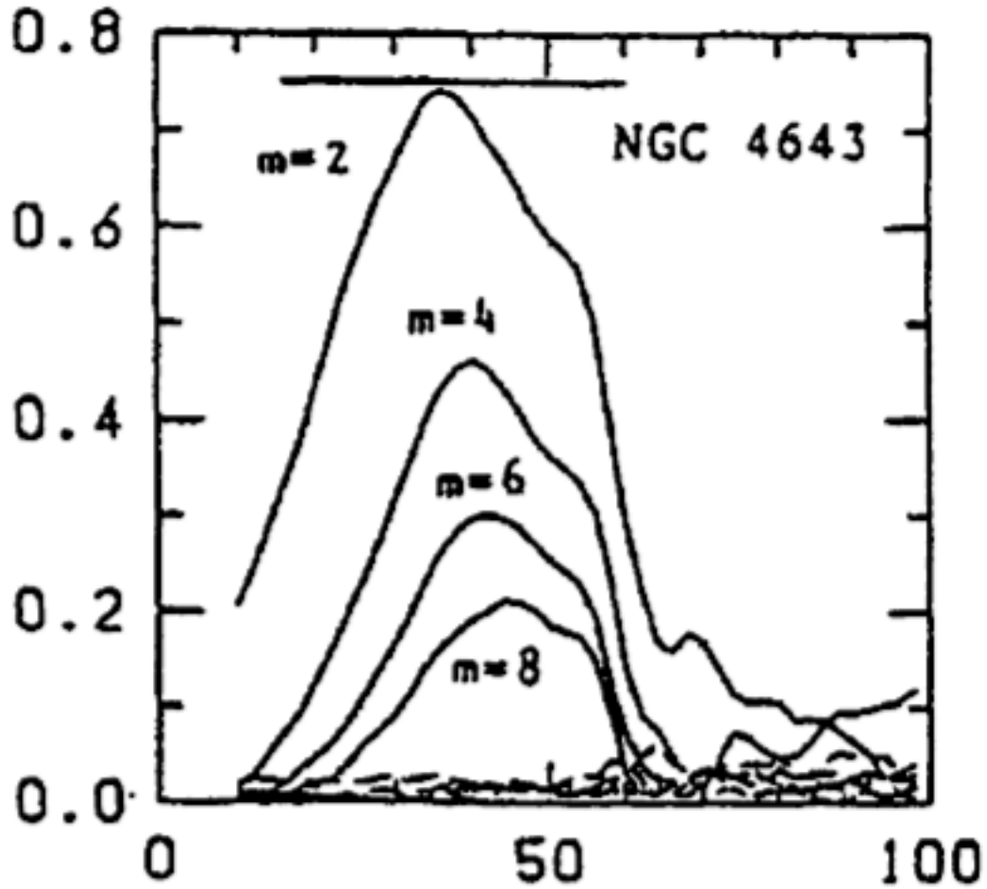

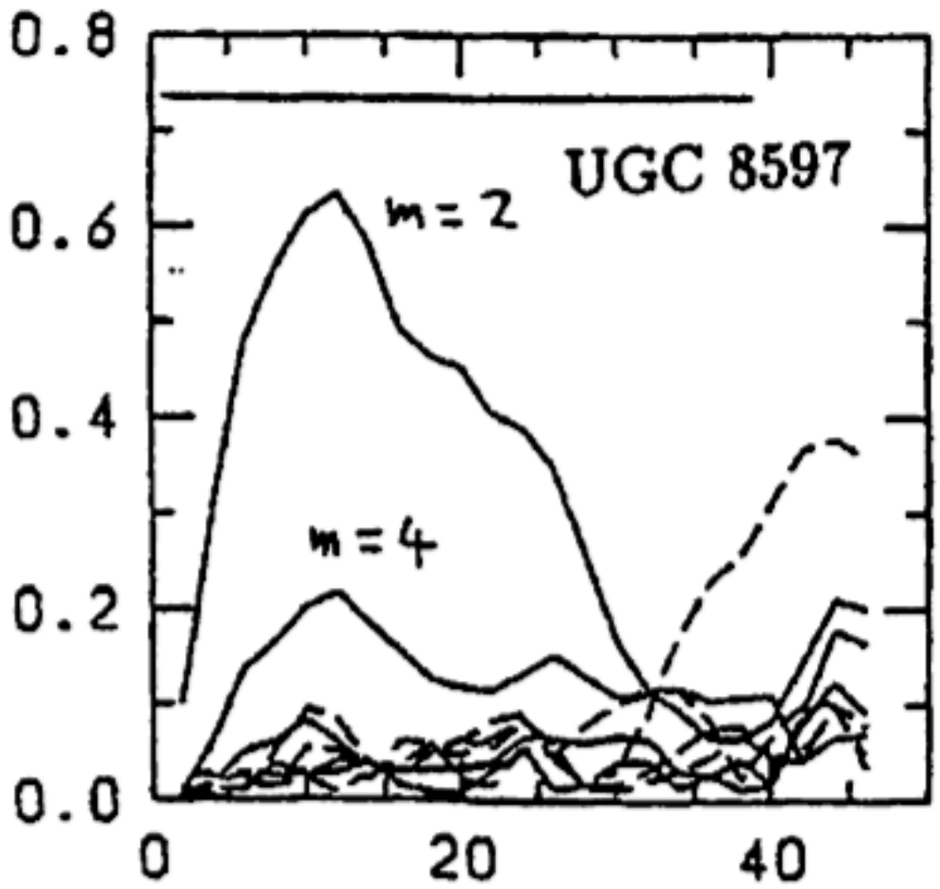

Figure 2. Relative Fourier amplitude of an early-type (left panel) and a late-type (right panel) barred galaxy. The ordinate is the relative amplitude of the Fourier component and the abscissa is radius in arcsec. A horizontal line in each panel represents a bar region.

Boxy shapes of isophotes

NGC1300

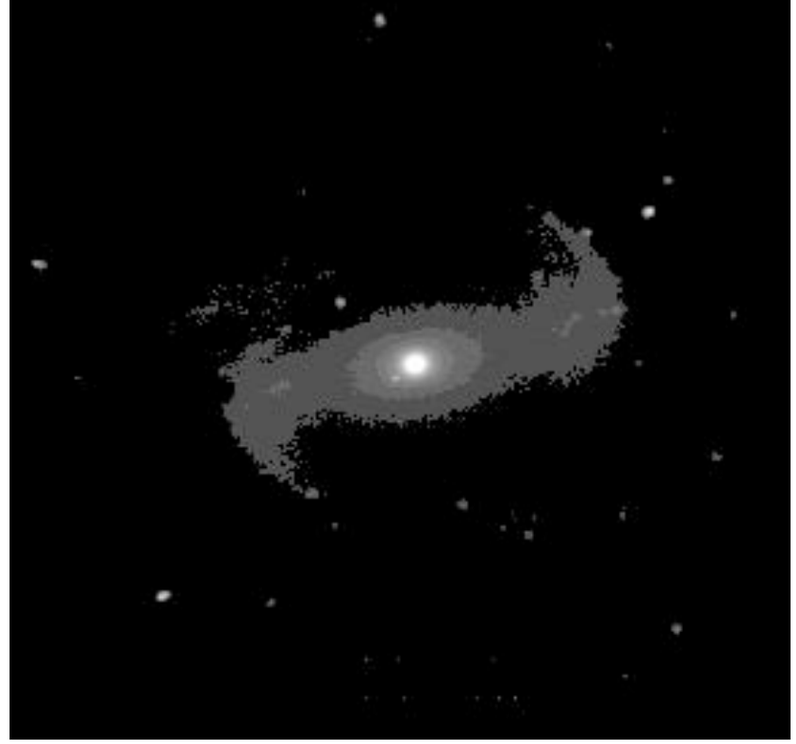

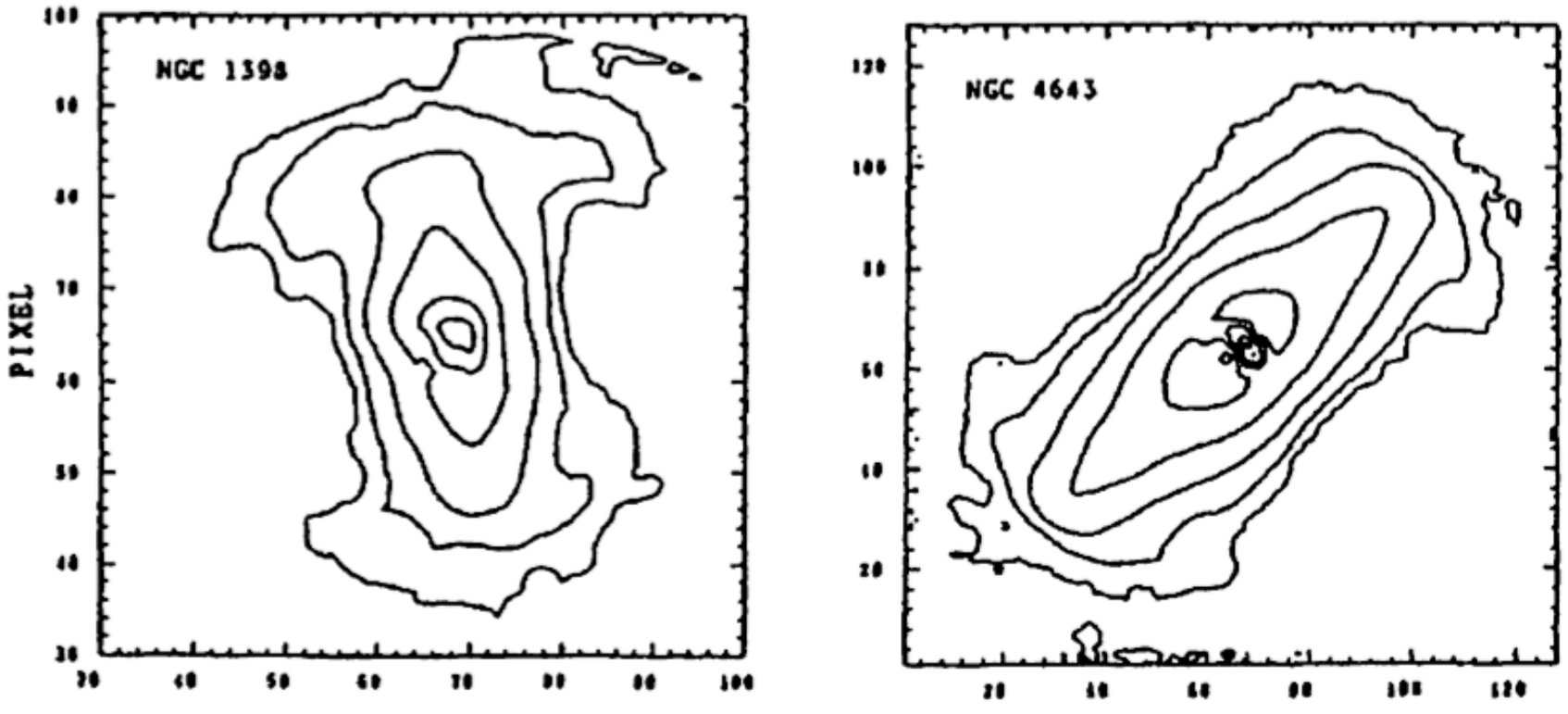

Figure 4. Examples of the isophotal map of the bar component itself in the early-type barred galaxies (NGC 1398 and NGC 4643). The outermost contour is 25.0 mag arcsec^{-2}, and the interval is 1.0 mag arcsec^{-2}.

NGC 3627

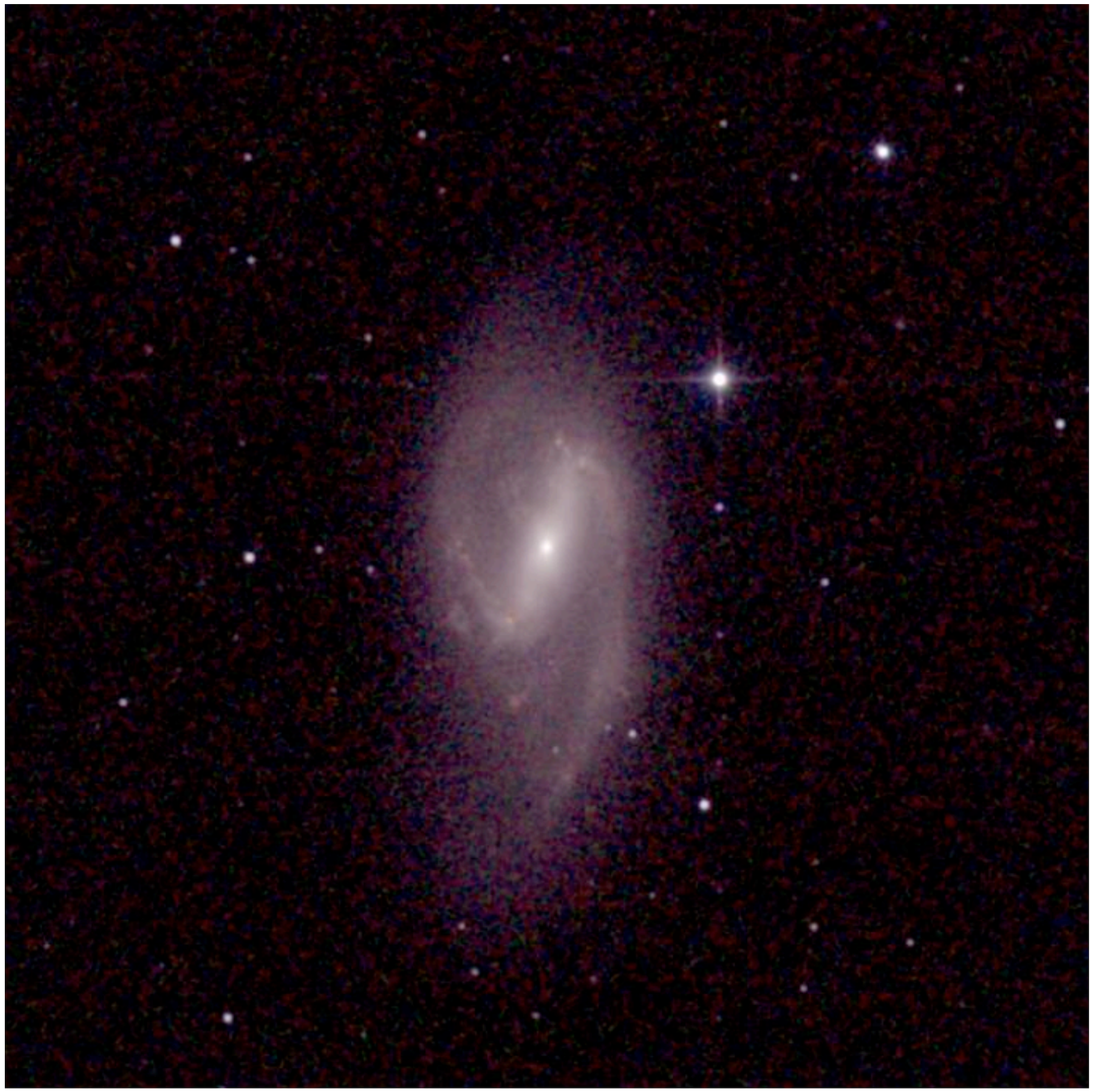

2MASS

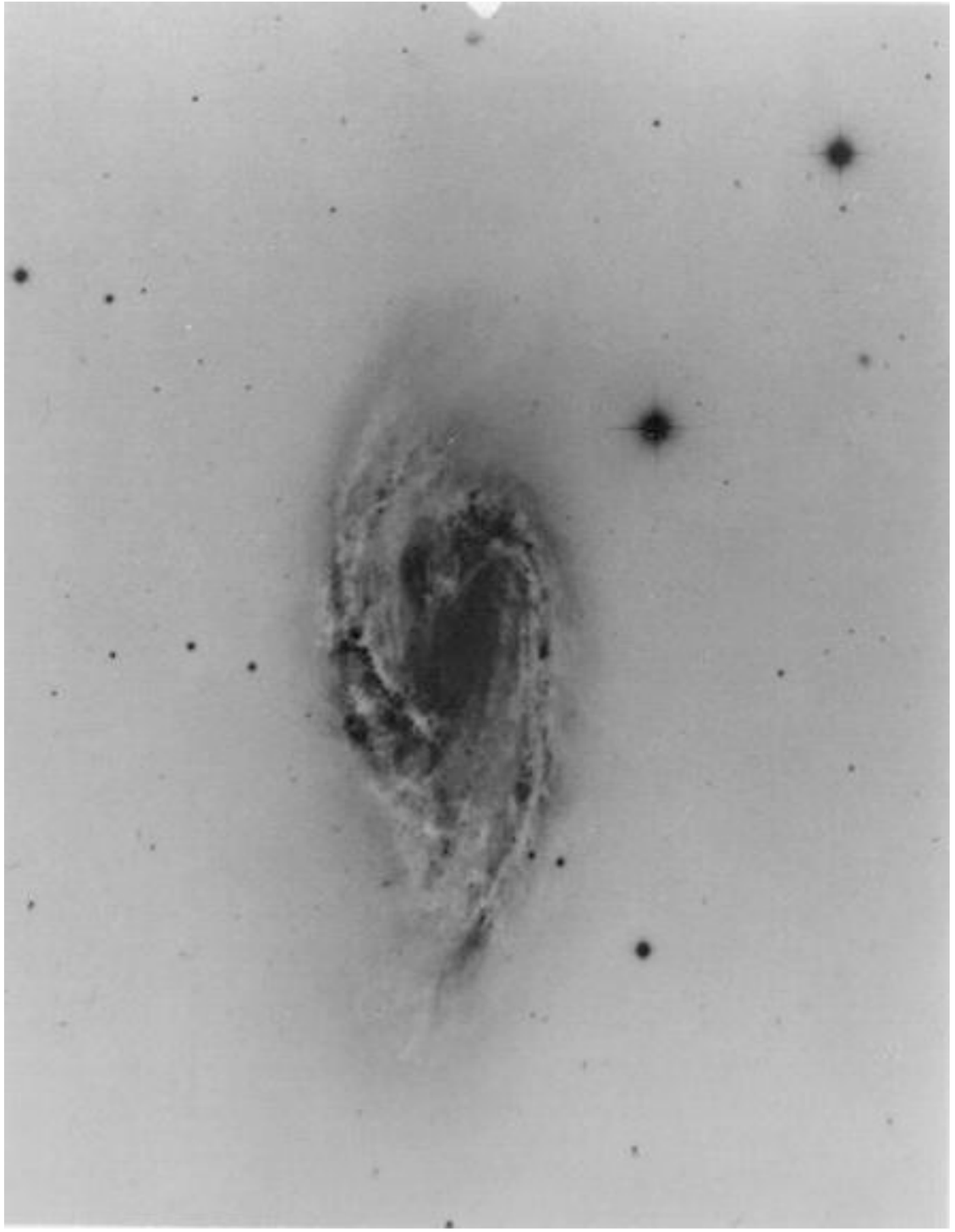

Palomar

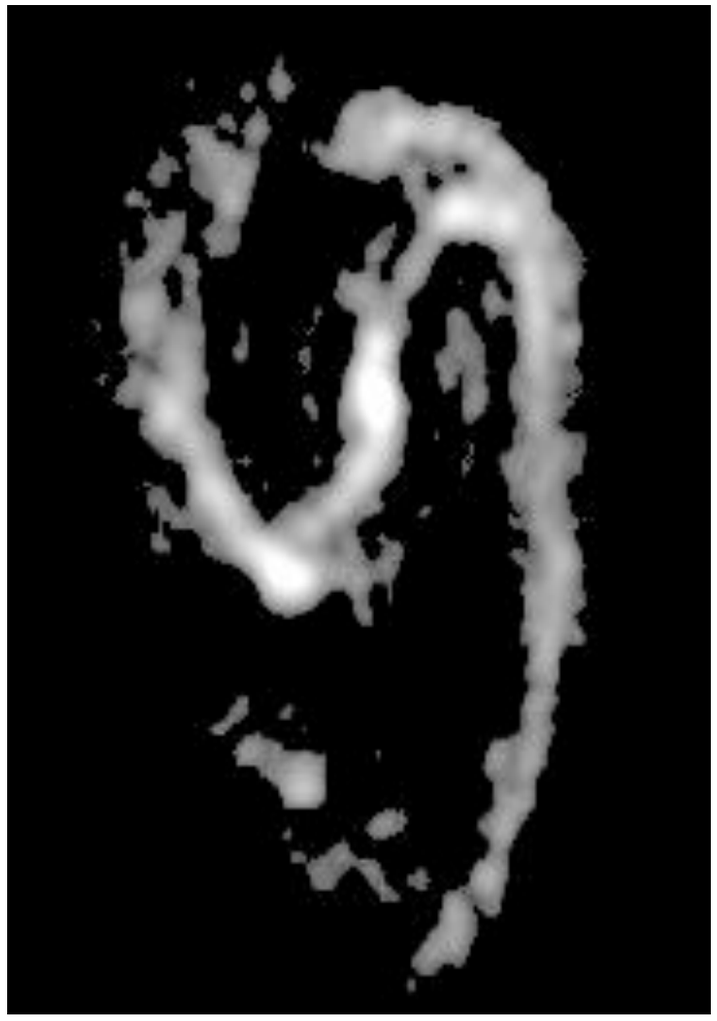

CO

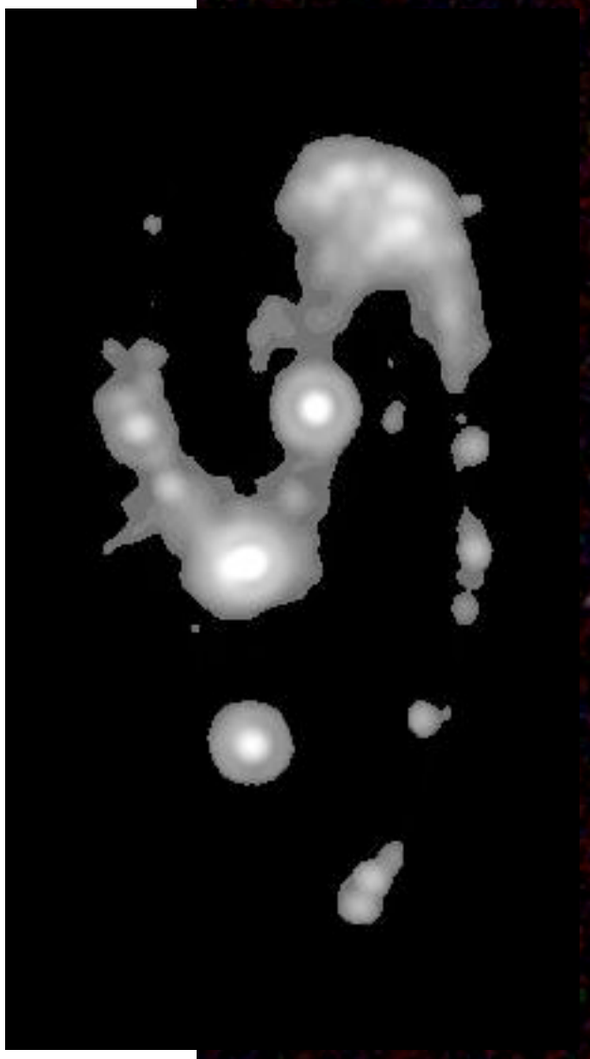

Spitzer (infrared)

2MASS: old stars

NGC 3627: different wavelengths

Star formation in barred galaxies

In general, global star formation rates and other properties are consistent with non-barred spirals of comparable Hubble class.

In barred spirals of intermediate class (SBb-SBc), the effects of the bar on star formation is clearly seen in the distribution of star forming sites. Two patterns: (a) star formation in rings (inner and nuclear rings for early-type bars) and (b) star formation in bar itself for late-type bars

Disk 1.8K Halo 10K Disk 18K Halo 100K Disk 180K Halo 1M

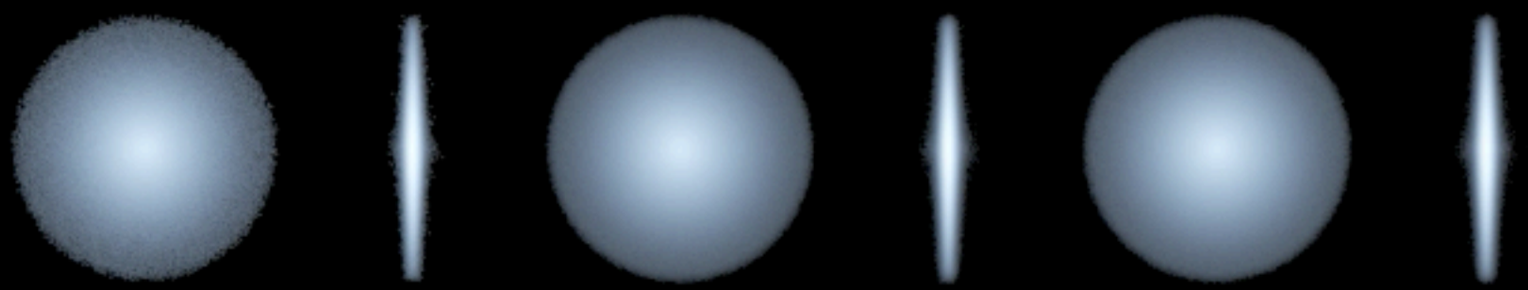

Disk 1.8M Halo 10M Disk 18M Halo 100M Disk 18M Halo 100M multi

Step 00000 t= 0.00 Gyr

Different stages of bar evolution

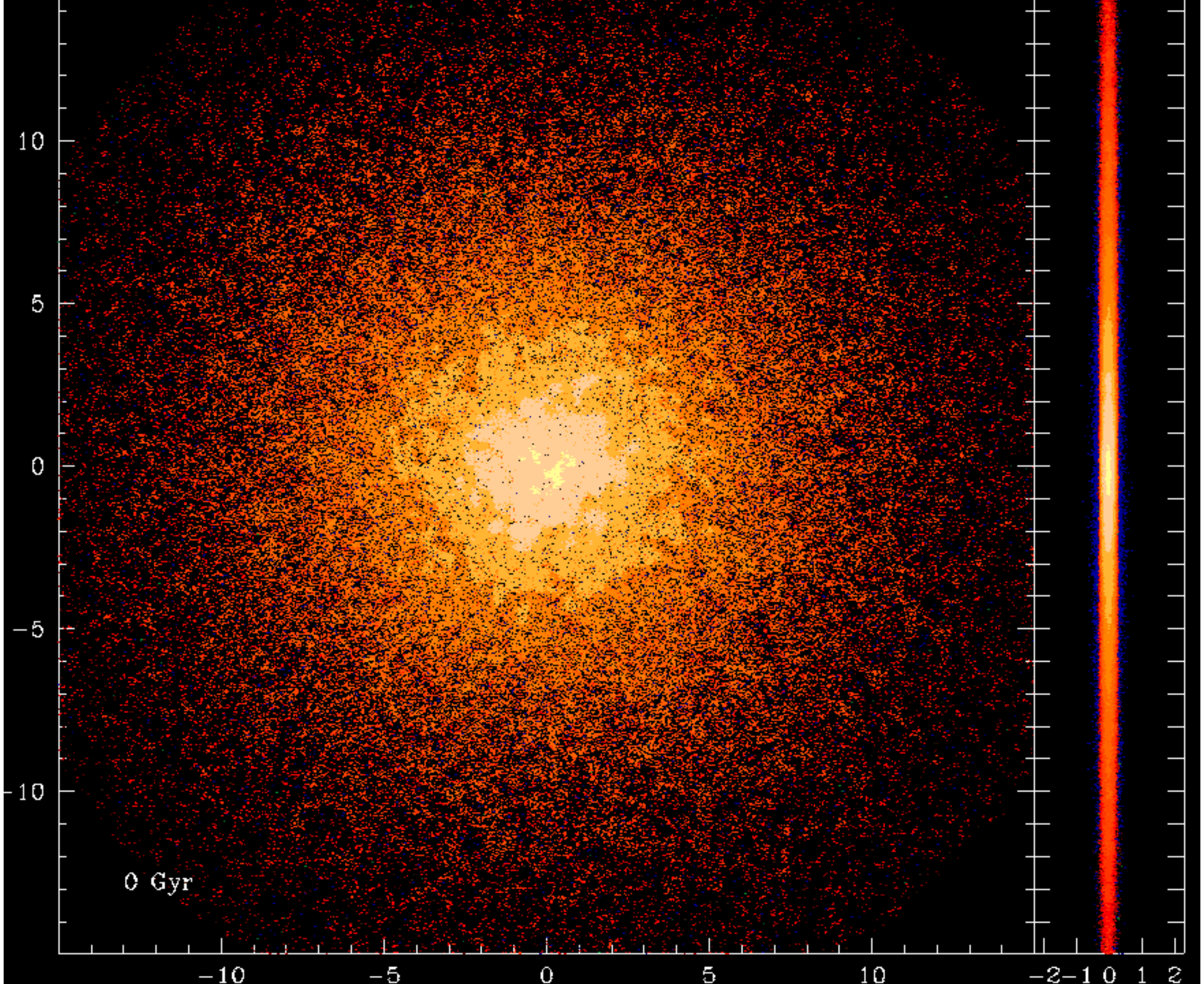
10
5
0
−5
−10
0 Gyr
−10
−5
0
5
10
−2
−1
0
1
2

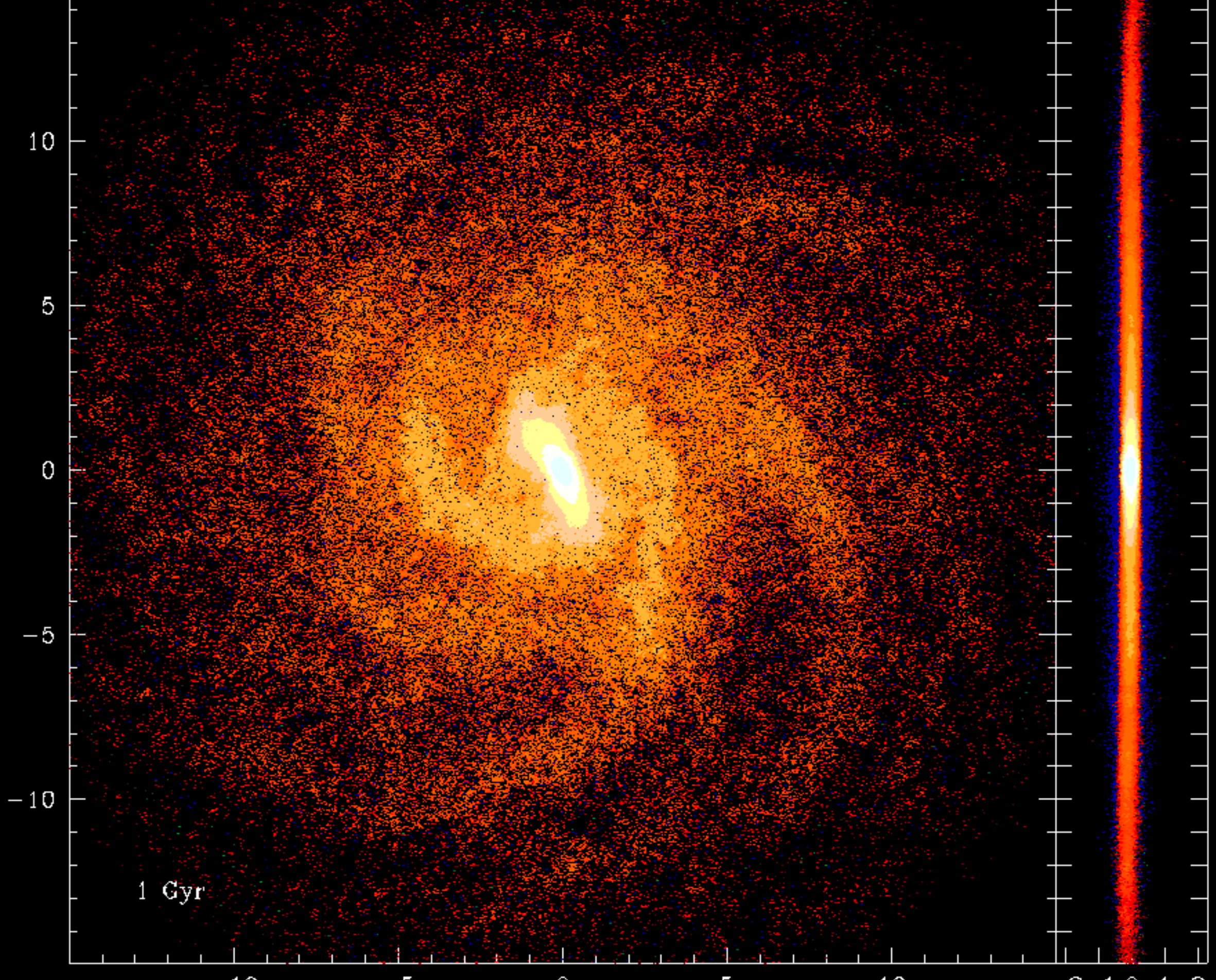
10
5
0
−5
−10
1 Gyr
−10
−5
0
5
10
−2
−1
0
1
2

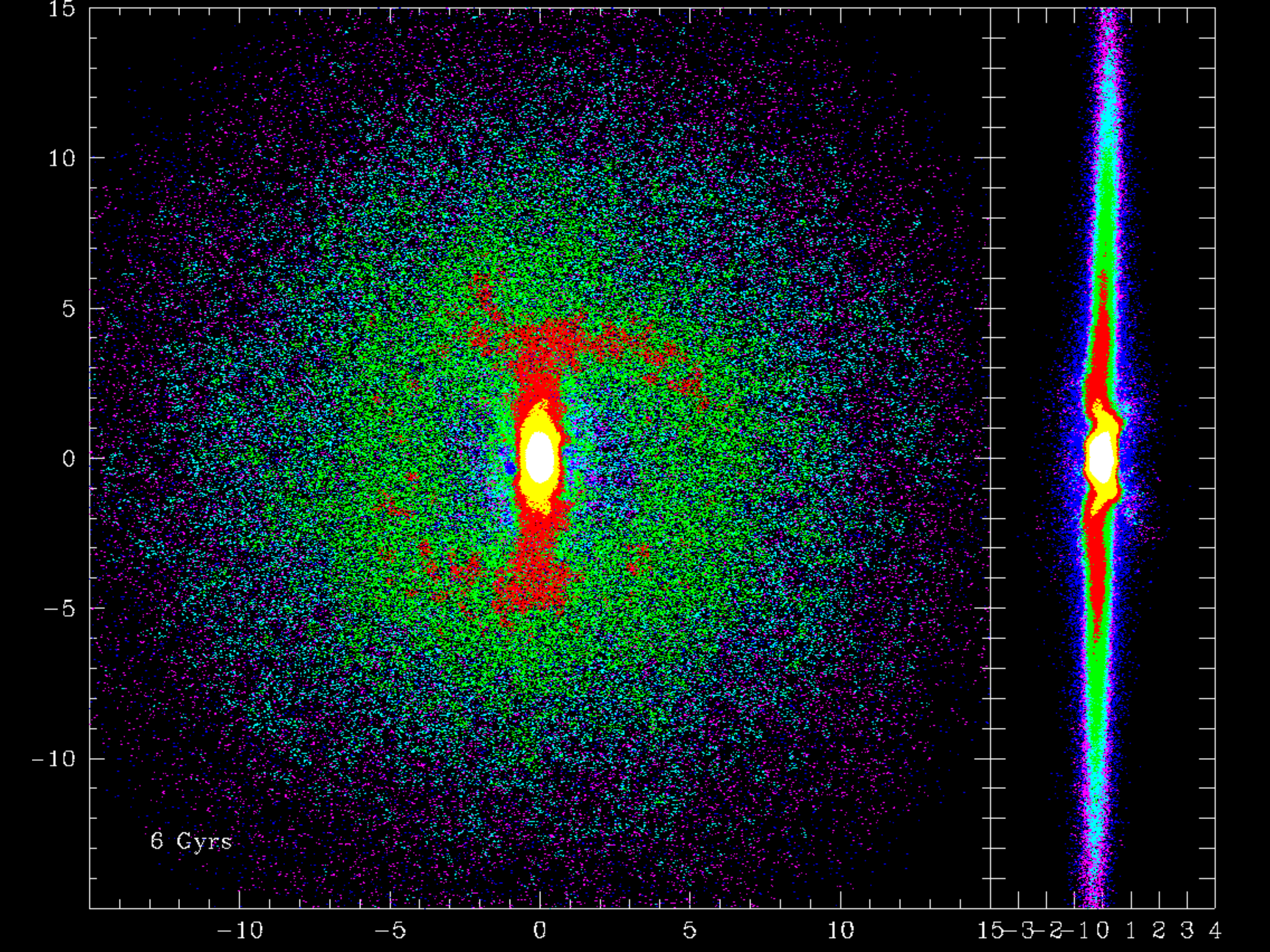
15
10
5
0
−5
−10
6 Gyrs
−10
−5
0
5
10
15
−3
−2
−1
0
1
2
3
4

Matching Milky Way

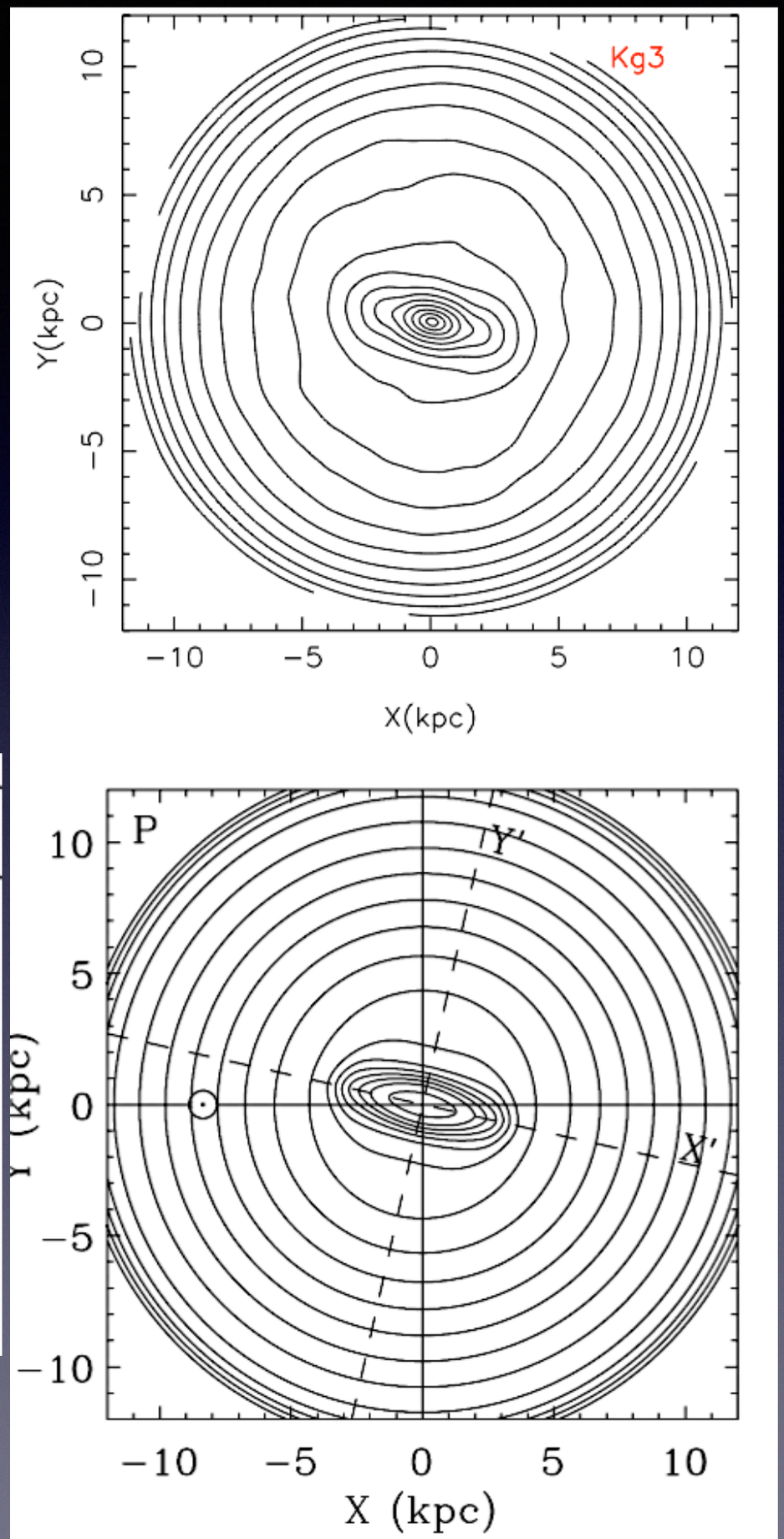

Parameter	K_{g3}	Milky Way
Circular velocity (km/s)	220	210-230
Surface disk density at $R_\odot$ $(M_\odot/pc^2)$	44.6	48 ± 9
Vertical rms velocity of stars at $R_\odot$ (km/s)	14	15-20
Radial rms velocity of stars at $R_\odot$ (km/s)	38	35-40
Pattern Speed Ω_p (km/s/kpc)	50	53 ± 3
Bar length (kpc)	3.3	3.0-3.5
Total mass inside 60 kpc $(10^{11} M_\odot)$	5.5	4 ± 0.7
Total mass inside 100 kpc $(10^{11} M_\odot)$	7.3	7 ± 2.5

Klypin et al 2009

Conclusions

- Realistic models of LCDM DM halos + stellar disk make sensible models for the MW
- More physical models (with 3D hydro, star formation, cooling/heating) now can be made.

Fast bars in DM halos

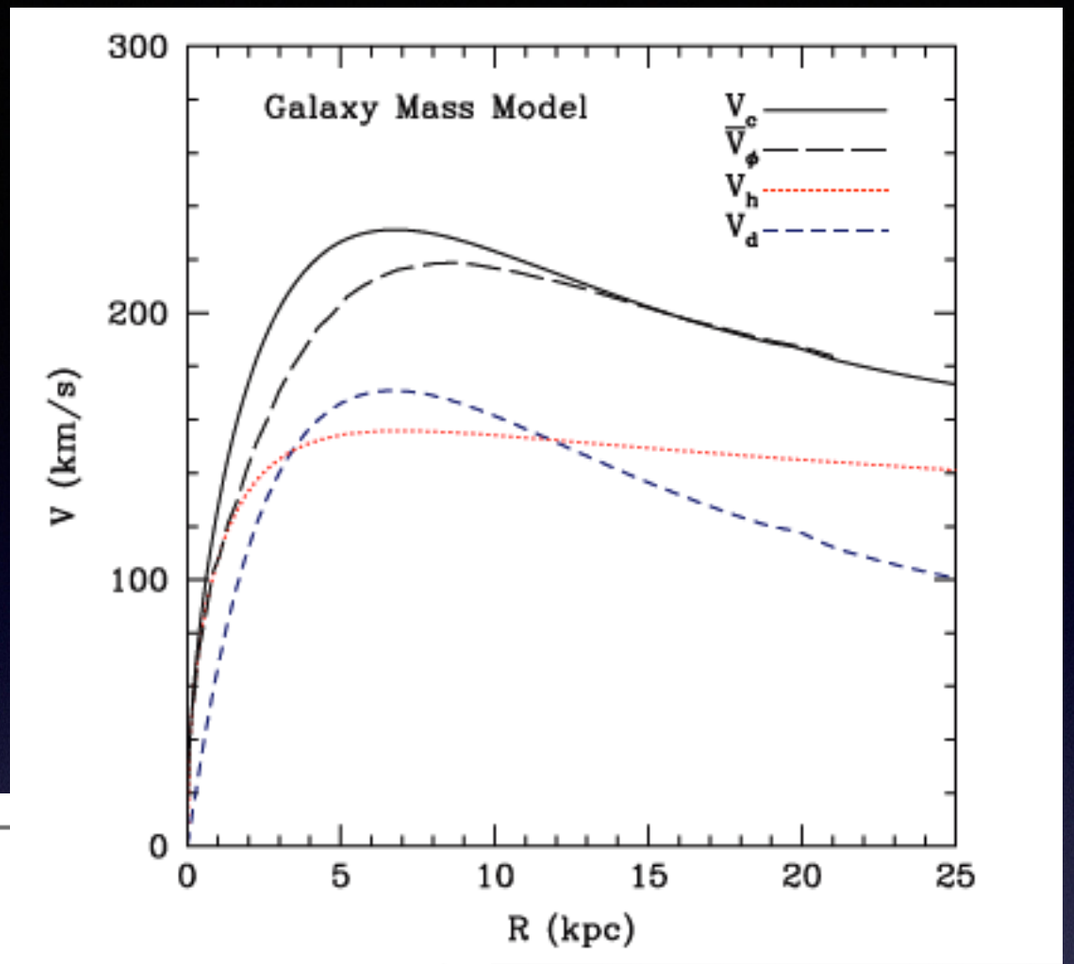

Dubinski et al 2009

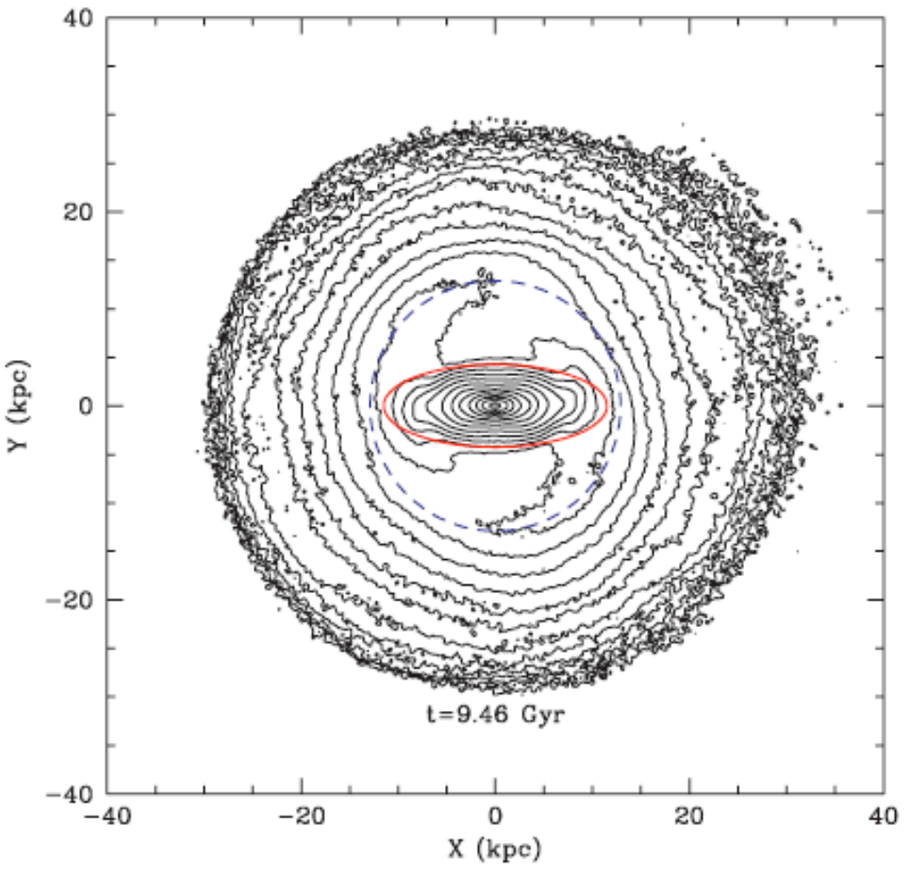

Figure 19. Surface brightness contours of the multimass model at the last snapshot at $t = 9.4$ Gyr overlayed with the best fit ellipse to the central bar and CR radius. Even at this late time in the evolution, the bar extends to the CR radius.

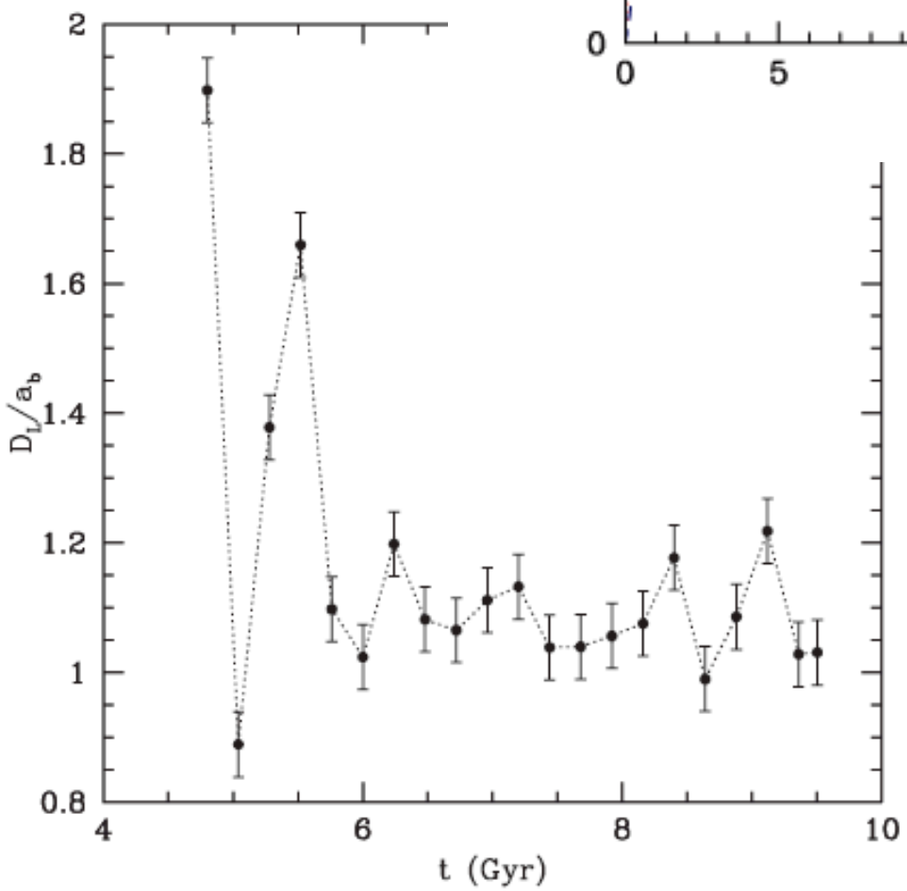

Figure 20. Evolution of the CR radius to bar length ratio $\mathcal{R} = D_L/a_b$ for the multimass model over the last half of the simulation. The value of $\mathcal{R}$ hovers around 1.1 indicating a fast bar.